02

Tunneling spectroscopy of underdoped $NaFe_{1-x}Co_xAs$ pnictides in the normal state

© I.A. Nikitchenkov[1,2], S.A. Kuzmichev[1,2], A.D. Ilina[2], I.V. Morozov[3], A.I. Shilov[2], E.O. Rakhmanov[3,2], T.E. Kuzmicheva[2]

[1] Faculty of Physics of Lomonosov Moscow State University, Moscow, Russia
[2] Lebedev Physical Institute, Russian Academy of Sciences, Moscow, Russia
[3] Department of Chemistry, Lomonosov Moscow State University, Moscow, Russia

E-mail: nikitchenkov.ia19@physics.msu.ru

Received March 6, 2025
Revised March 6, 2025
Accepted May 5, 2025

Single crystals of underdoped $NaFe_{0.979}Co_{0.021}As$ pnictides (i. e., with a deficiency of substituting cobalt compared to the compound possessing the maximum critical temperature T_c) were studied using tunneling spectroscopy in the superconducting and the normal state. The obtained $dI(V)/dV$-characteristics of tunneling contacts reproducibly showed residual nonlinearity both below and above the critical temperature. This nonlinearity, being unusual for conventional tunneling junction, was not directly related to the superconducting properties and disappeared at $T \approx 60$ K. Possible origin of this nonlinearity and its potential relation with the nematicity of the electronic subsystem are discussed.

Keywords: high temperature superconductivity, iron arsenide, break-junction, phase diagram.

DOI: 10.61011/PSS.2025.07.61875.11HH-25

1. Introduction

The cobalt-doped compounds $NaFe_{1-x}Co_xAs$ belong to the 111 family [1,2], an extensive class of iron-containing high-temperature superconductors (HTSC) [3]. The crystal structure of the 111 family is quasi-two-dimensional and contains superconducting $FeAs^-$ layers located perpendicular to the crystallographic axis c and separated by a layer of alkali metal cations Na^+.

The electronic structure of NaFeAs exhibits a pronounced quasi-two-dimensional character. There are hole cylinders near the Γ-point of the Brillouin zone and electron cylinders near the M-point on the Fermi surface [4], where several superconducting condensates are formed below the critical temperature of transition to the superconducting state T_c (see Figure 9 in Ref. [5]). It is interesting to note that some papers [6,7] reported an anomalous change in the electronic structure of iron-containing HTSCs with an increase in temperature at $T > T_c$, which is unusual for classical concepts.

Unlike representatives of the 1111 and 122 families, superconductivity in the pnictides of the 111 family is found for the stoichiometric composition of NaFeAs. In addition to the superconducting phase, NaFeAs demonstrates a structural phase transition from tetragonal syngony (P4/nmm) to orthorhombic syngony (Cmma) at $T_s \approx 55$ K followed by antiferromagnetic (AFM) ordering at $T_m \approx 43$ K to a spin density wave state, while the AFM and superconducting phases are separated by crystal volume in undoped compositions (for an overview, see Ref. [5]). The structural transition at $T_s > T_m$, on the one hand, as noted in Ref. [8], correlates with the properties of the electronic subsystem and may be due to orbital ordering. Even with a small substitution of Fe atoms by Co, the temperatures T_s and T_m decrease, tending to zero near the optimal doping region, and the critical temperature in the $NaFe_{1-x}Co_xAs$ system reaches a maximum value of $T_c \approx 22$ K at the substitution level $x = 0.03-0.04$ [9]. When x decreases or increases, the dependence $T_c(x)$ in HTSC compounds usually circumscribes the „superconducting dome“, going into the so-called „underdoped“ or „overdoped“ region on the phase diagram, respectively.

The nematic order of the electronic subsystem is defined as a spontaneous breaking of the C_4-symmetry [10,11] and is accompanied by the appearance of anisotropy of some transport, magnetic and optical properties in the ab-plane of [12–17]. It should be noted that the nematicity of the electron subsystem was observed up to temperatures much higher than T_s in materials of the NaFeAs family in some studies [12,14,15]. Nematic fluctuations also cover the region of the phase diagram beyond the structural transition [18]. A similar breaking of the C_4-symmetry of the properties of the electronic subsystem has been observed in other superconductors of underdoped compositions, where the magnetism of iron (and, possibly, nematicity) coexist with superconductivity [19,20]. On the contrary, the

observation of nematicity has not been reliably confirmed in „magnetic“ superconductors of the $EuRbFe_4As_4$ family, where the long-range magnetic order is lower than T_c due to the magnetism of 4f orbitals of Eu [21,22].

According to calculations in Refs. [23,24], a superconducting order parameter with the C_2-type symmetry is realized below T_c against the background of the nematic electronic subsystem. For example, this was confirmed experimentally using quasiparticle interference in FeSe [25].

The question of the nature of the nematic state remains open [11]. Thus, the relationship of nematicity with spin, charge, orbital, and superconducting subsystems is discussed in Refs. [8,24–28]. In the general case, three order parameters are implemented in the nematic state [11]: 1) structural ordering, directly related to the distortion of the crystal lattice by phonons; 2) charge/orbital ordering, related to the nonequivalence of the filling of d_{xz}- and d_{yz}-orbitals; 3) spin ordering, resulting from the nonequivalence of peaks of dynamic spin susceptibility $\chi(q, \omega)$ on vectors $(\pi, 0)$ and $(0, \pi)$. It is not possible to prove strictly which of the above orders is primary and, consequently, which type of fluctuations is a precursor of nematicity, either theoretically or experimentally [11].

One of the interesting features of the band structure of some iron-containing HTSC of predominantly underdoped compositions is the „mini-gap“ below the Fermi level E_F and the presence of van Hove singularities at its edges [29] associated with the asymmetry of bands formed by $3d_{xz}$- and $3d_{yz}$-orbitals of iron, in the nematic phase at temperatures exceeding T_s [30,31]. The presence of electron density of state peaks $N(E)$ near E_F and their smoothing with increasing temperature at $T > T_s$ was predicted in Ref. [26]. Similar results were obtained in Ref. [32] for NaFeAs and $BaFe_2As_2$ of stoichiometric compositions.

In experiments using angle-resolved photoemission spectroscopy (APRES), a noticeable temperature change in spectral density near the Fermi level was observed mainly in superconductors of stoichiometric and underdoped compositions (i. e., near the AFM and nematic phases): in NaFeAs [16,33], $NaFe_{0.9825}Co_{0.0175}As$ [34] and pnictides of the Ba-122 family [30,31]. The nonmonotonicity of $N(E)$ in the pnictides of the Ba-122 family is indirectly confirmed by the observation of the residual nonlinearity of the dynamic conductance spectra of tunneling contacts in the normal state above T_c [35–38], a minimum of $dI(V)/dV$ was observed at zero bias in these studies. On the contrary, the authors of theoretical papers [39,40] predict the occurrence of a logarithmic term in the nematic phase near E_F to the single-particle function $N(E)$, which leads to the appearance of a peak of dynamic conductance at zero bias on the $dI(V)/dV$-spectrum of the tunneling contact [40]. Based on the predictions in Ref. [40], the authors of the study in Ref. [38] associate the observed transformation of the minimum $dI(V)/dV$ into a maximum occurring with the temperature increase to the nematic phase. However, the reasons why the $dI(V)/dV$-spectrum at low temperatures in the region of $T > T_c$ demonstrates a lack of conductance at zero bias remain unclear [38].

This paper is devoted to the study of the properties of $NaFe_{1-x}Co_xAs$ ferropnictides of underdoped composition $(x = 0.021)$ by tunneling spectroscopy, which allows local study of the bulk properties of the electronic subsystem. Earlier, when studying the superconducting order parameter in $NaFe_{1-x}Co_xAs$ [41], our group discovered features in tunneling $dI(V)/dV$-spectra at large biases $eV > 2\Delta_L(0)$, where $\Delta_L(0)$ is the magnitude of a large superconducting gap at zero temperature. These anomalies, which are not directly related to the superconducting state, were observed at $T > T_c$. This paper reveals the temperature evolution of these features of the normal state over a wide temperature range. Based on the experimental data obtained, an analysis of the possible causes of the investigated nonlinearity is carried out. The nature of the observed effect is discussed.

2. Details of the experiment

Samples of nominal composition $NaFe_{0.979}Co_{0.021}As$ were grown by crystallization from a melt containing a small excess of As. The details of the synthesis, as well as the characterization of the single crystals used using X-ray spectral analysis, measurements of the temperature dependences of resistance $R(T)$ and magnetization $M(T)$ are discussed in detail in Refs. [41,42]. The data obtained confirm the homogeneity of the composition of the synthesized single crystals and the presence of a single superconducting phase with $T_c^{onset} \approx 20.5$ K. The composition of the grown single crystals $Na_{0.69(3)}Fe_{1.048(11)}Co_{0.0094(9)}As_{1.000(12)}$ was determined as a result of joint statistical processing of energy dispersion spectroscopy data obtained in 8–10 points on the surface of five crystals.

A mechanically controlled planar modification [43] of the break-junction technique (MCPBJ) [44] was used to obtain tunneling structures of the ScS type (where S is a superconductor, c is a constriction) and NcN (N is a normal metal). Within the framework of this technique, a tunneling contact is created on a microcrack resulting from mechanical splitting of a single crystal at low temperatures $T = 4.2$ K.

$NaFe_{1-x}Co_xAs$ rapidly degrades in the air atmosphere due to the presence of an alkali metal in the structure, therefore, all manipulations with the test sample during preparation for measurements were performed in a glove box with a dry argon atmosphere. Within the methodology, a rectangular single crystal sample of the layered $NaFe_{1-x}Co_xAs$ compound, shaped as a thin plate with typical dimensions of $3 \times 1.5 \times 0.1$ mm^3, was mounted on the surface of a U-shaped elastic holder such that the ab-plane of the crystal coincided with the plane of the holder. Subsequently, electrical contacts were established in a four-point measurement configuration using In-Ga solder drops placed on the corners of the single crystal. The holder

and the sample were cooled to a temperature of $T = 4.2\,\mathrm{K}$, while In-Ga solidified and mechanically fixed the single crystal on the surface of the holder. Under the influence of the displacement of the micrometer screw, the holder bends precisely, which leads to exfoliation of the single crystal in the ab-plane with the formation of tunneling contact on natural steps and terraces separating two cryogenic clefts along the c-direction (Figure 1 in Ref. [45]). In this way, a tunneling contact with pure cryogenic clefts is formed, and the measurement current always flows through the contact along the c-direction. The moment of occurrence of cryogenic clefts is controlled by the appearance of the finite slope of the current-voltage characteristic (CVC) in real time. Further mechanical adjustment of the bending of the holder during the experiment allows adjusting the geometry of the tunneling contact by changing its area, while the bulk energy parameters are studied locally.

In the superconducting state (below T_c), the obtained symmetrical tunneling ScS contacts demonstrated a number of spectral features that allowed them to be classified as SNINS-type with high transparency of weak link (I — insulator with barrier parameter $Z < 0.3$), the lack of phase coherence between S-banks and a semiballistic transport ($l > d \gg \xi_0$, where l is the mean free path, d is the contact size, both values are taken in crystallographic ab-direction; ξ_0 is the coherence length). In accordance with the theoretical concepts described in Refs. [45–48], the effect of Andreev reflections realized in such a contact causes Andreev excess current over the entire range of bias V, the peak of differential conductance of the contact G_{ZBC} at small voltage bias of $V \to 0$ (so called „foot“), as well as features in case of a bias of $eV(T) = 2\Delta(T)$. Formally, regardless of the value of Z, transport through such a ScS contact can be called „tunneling“ of carriers using the processes of Andreev scattering and direct transmission.

Inelastic processes shorten the lifetime of Cooper pairs and quasiparticles by broadening the peaks of the density of states $N(E)$ in both the superconducting and normal states. The degree of smearing is characterized by the energy parameter $\Gamma = \hbar/(2\tau)$, introduced by Dynes [49], and is reflected in the tunneling experiment as a broadening of the observed spectral features [50]. Experimentally [51], an abnormally high amplitude of inelastic scattering (smearing parameter) $\Gamma \approx \Delta(0)$ and its non-fermi liquid behavior ($\Gamma \propto E$) were shown for the related LiFeAs compound. The presence of an insulator in barrier c (which corresponds to $Z \neq 0$) is an additional factor reducing the magnitude of the Andreev excess current at $eV \gg 2\Delta$ and Andreev conductance at zero bias [46,47].

The superconducting contact banks turn to the normal state at $T > T_c$. In accordance with the phenomenological approach of Giaever and Megerle [52], the current through a symmetrical N′cN contact is determined by renormalizing the density of electronic states $N(E)$ near E_F:

$$I(V) = A' \int_{-\infty}^{\infty} N'(E)N(E+eV)\{f(E) - f(E+eV)\}dE, \tag{1}$$

where A' is the contains a geometric factor and a tunneling matrix element, $f(E)$ is the Fermi-Dirac equilibrium distribution. This approach is usually used to describe contacts with low transparency ($Z > 3$), and the approach of the Blonder-Tinkham-Klapwijk (BTK) [46] model can be used for $E \gg \Delta \to 0$ for a barrier with an arbitrary Z. In particular, the following expression for tunneling current is obtained using the BTK model for the N′cN contact (above T_c):

$$I(V) = \frac{1}{eR_N} \int_{-\infty}^{\infty} T(E)\{f(E) - f(E+eV)\}dE, \tag{2}$$

where the transmission probability

$$T(E) = 1 - B(E) = 2N(E)/[N(E) + 1 + 2Z^2]. \tag{3}$$

In the quasiclassical case, when there are no van Hove singularities near the Fermi level and the dimensionless $N(E) \approx \mathrm{const}$, the CVC of the NcN contact has an ohmic (linear) shape. On the contrary, if the function $N(E) \neq \mathrm{const}$ is near E_F — for example, due to the features of the band structure (at any temperature) or due to the renormalization of the density of electronic states for interaction with bosonic modes characteristic of the system below T_c — CVC of the studied contact deviates from the ohmic dependence. In this case, by examining the nonlinearity of the CVC, it is possible to obtain some information about the behavior of the function $N(E)$ in this compound. The effect will also be observed for high transparency contact with small Z, according to formulas (2) and (3), however, the amplitude of the nonlinearity of the $dI(V)/dV$-spectrum will be less than the amplitude of the $N(E)$ change.

3. Results

Figure 1 shows the CVC (a) and the corresponding differential conductance spectra (b) of tunneling contacts created in the $NaFe_{0.979}Co_{0.021}As$ sample using the planar „break-junction“ technique. The red curves correspond to temperature $T = 4.2\,\mathrm{K}$, whereas the blue curves were obtained in the normal state at temperature $T = 22.4\,\mathrm{K} > T_c$. In accordance with all available theoretical approaches [45–47], below T_c, the tunneling contacts shown in Figure 1 are in an incoherent SNS regime: in the superconducting state, there is no supercurrent branch on the CVC, there is an excess current I_{exc} over the entire range of bias voltages (dark yellow curve, Figure 1, a)), as well as the „foot“ with an amplitude of G_{ZBC} at low bias.

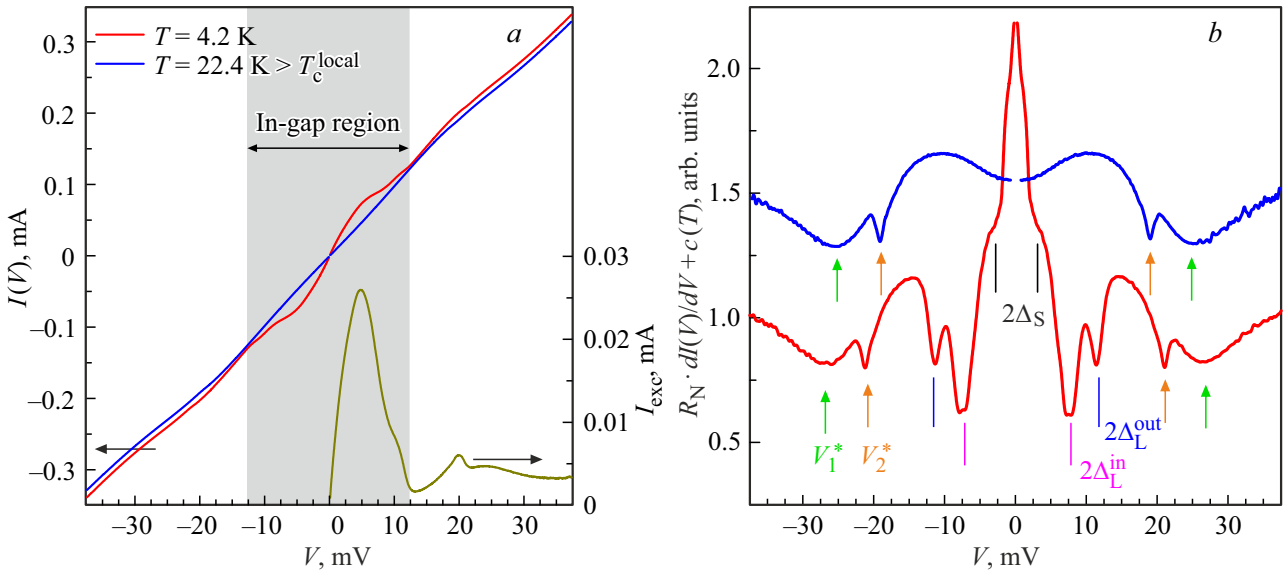

Figure 1. *a* — CVC of the tunneling contact measured at $T = 4.2$ K (ScS, red line) and above T_c at $T = 22.4$ K (NcN, blue line). The insert shows the Andreev excess current $I_{exc}(V) \equiv I(V, 4.2\,\text{K}) - I(V, 22.4\,\text{K})$ (dark yellow line). The in-gap bias area is marked in gray. *b* — $dI(V)/dV$ is the spectrum of this contact, measured at $T = 4.2$ and 22.4 K (lines of corresponding colors). The spectra are manually shifted vertically for convenience. Vertical dashes at $T = 4.2$ K mark the position of the fundamental Andreev features of three SC order parameters of $2\Delta_L^{out} \approx 11.3$ meV, $2\Delta_L^{in} \approx 7.5$ meV, $2\Delta_S \approx 2.6$ meV. The arrows show the position of the characteristic minima of the residual nonlinearity of the $dI(V)/dV$-spectrum, which is not directly related to the SC properties: $V_1^* \approx 26.6$ mV, $V_2^* \approx 21.2$ mV.

The in-gap region of the obtained $dI(V)/dV$-spectrum (red curve in Figure 1, *b*) contains three main features at biases $|V| \approx 11.3, 7.5$ and 2.6 mV below T_c, defining three characteristic energies for the superconducting order parameter and indicating its anisotropy: $2\Delta_L^{out}$, $2\Delta_L^{in}$ and $2\Delta_S$, respectively. Similar Andreev structures have been analyzed in more detail in previous papers [41,42]. $2\Delta_L^{out}$ and $2\Delta_L^{in}$ have similar temperature dependence and presumably belong to the same superconducting condensate, which is anisotropic in k-space, being the maximum and minimum coupling energies of Cooper pairs depending on the direction of the momentum; on the contrary, a small superconducting gap $2\Delta_S$ demonstrates distinct temperature dependence and opens up in other bands below T_c [42].

The features caused by the effect of Andreev reflections on the CVC and the differential conductance spectrum in Figure 1 disappear in case of transition to the normal state. However, the $I(V)$ and $dI(V)/dV$ characteristics demonstrate a general (residual) nonlinearity over a large bias range above T_c. The spectrum exhibits minima at $V_1^* \approx 26.6$ mV, $V_2^* \approx 21.2$ mV, indicated in Figure 1, *b* by arrows. The minimum at $eV = 0$ on the blue curve is not reproduced for the contacts we obtained based on $NaFe_{1-x}Co_xAs$ and may be in this case a consequence of heating the contact area with a measuring current. It should be noted that the spectra in Figure 1, *b* are manually shifted vertically for convenience of consideration: in fact, the dynamic conductance G_N of the contact at large bias $eV \gg \Delta(0)$ did not change with the increase of the temperature.

The detected nonlinearity of the normal state is reproduced from contact to contact. Figure 2 contains a set of data measured at $T > T_c$ CVC (*a*) and $dI(V)/dV$-spectra (*b*). It is interesting to note that although the data in Figure 2 are measured in the normal state, the characteristics shown resemble $I(V)$ and the spectra of NIS contacts obtained in the superconducting state, this is nevertheless an imitation. We have obtained tunneling contacts of different areas with significantly different normal resistance $R_N = 1/G_N$, which can be estimated from the slope of the CVC in the region $eV \gg \Delta(0)$. Regardless of the size of the contact, the characteristic shape of the studied residual nonlinearity of the normal state is reproducible: a maximum in the low-bias region, as well as two minima $dI(V)/dV$ at voltages V_1^* and V_2^*, highlighted in Figure 2, *b* with green and orange dashes, respectively. The characteristic positions of these two minima are also reproduced. The histogram of Figure 3, *a* shows the statistics of V_1^*, V_2^* values obtained on various samples of $NaFe_{1-x}Co_xAs$ undoped compounds with $T_c \approx 19-22$ K from the same batch. It can be seen that for the obtained contacts, on average, characteristic minima of nonlinearity are observed at $V_1^* \approx 20$ mV, $V_2^* \approx 27$ mV, and the spread of values does not exceed ±11%. This variation does not correlate with the resistance of the received contacts, as shown in Figure 3, *b*. The shown reproducibility does not allow attributing the studied features to random effects or geometric resonances occurring in the contact area. Thus, the observed residual nonlinearity of the $dI(V)/dV$-spectra

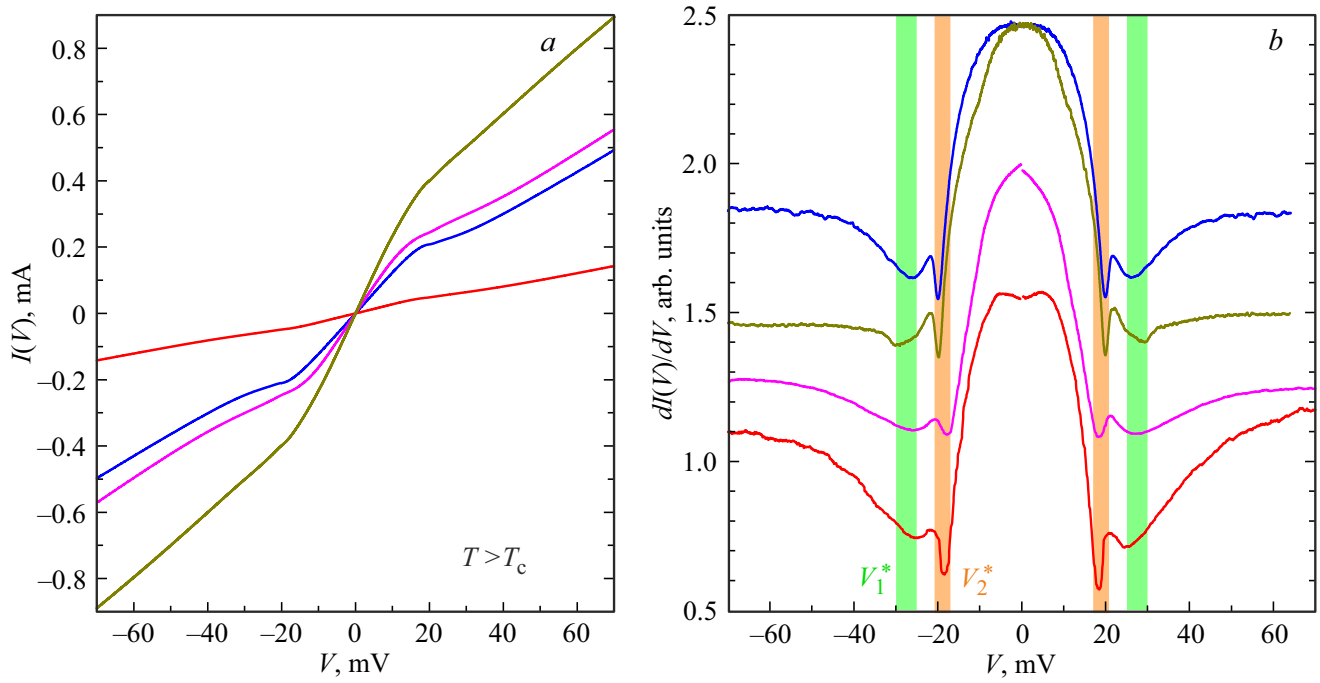

Figure 2. *a* — CVC and *b* — $dI(V)/dV$-spectra of NcN contacts measured in the normal state at $T > T_c$. The shape of these curves mimics the characteristics of the NS contact. The spectra are manually shifted vertically for convenience. Vertical lines mark the position of the characteristic minima of the residual nonlinearity of the $dI(V)/dV$ spectrum, which is not directly related to the SC properties: $V_1^* \approx 27.5$ mV, $V_2^* \approx 18.5$ mV.

is related to the internal, bulk properties of the normal state of the compound $NaFe_{1-x}Co_xAs$.

Figure 4, *a* shows $dI(V)/dV$-spectrum of the tunneling contact measured in the temperature range of $4.2\,K \le T \le 35\,K$, i. e. both in superconducting (ScS) and normal (NcN) states. As the temperature increases, the characteristic features of the Andreev reflection effect („foot“ at $eV = 0$, gap features) gradually smear; at the same time, the gap minima (marked at $T = 4.2$ K in vertical strokes) shift to the region of zero bias voltage, completely disappearing from the spectrum when T_c is reached. The temperature course of superconducting order parameters $2\Delta_L^{out}$ and $2\Delta_L^{in}$ (the assumed extremes of the large superconducting gap), represented by circles in Figure 4, *b*, is extracted from the position of the minima. The obtained temperature dependences $\Delta_L^{in,out}(T)$ are generally close to the corresponding dependence $\Delta(T)$, which is given by the Bardeen-Cooper-Schrieffer theory (represented by a solid line in Figure 4, *b*), but are slightly lower which can be explained by a moderate interband interaction (a detailed analysis of this dependence in the framework of the multiband approximation is given in Ref. [42]). The local critical contact temperature $T_c^{local} \approx 20.7$ K was estimated as the temperature at which the related BCS-like fit turns to zero.

On the contrary, the shape of the residual nonlinearity of the $dI(V)/dV$-spectra in the normal state changes less with increasing temperature (Figure 4, *a*). The positions of the

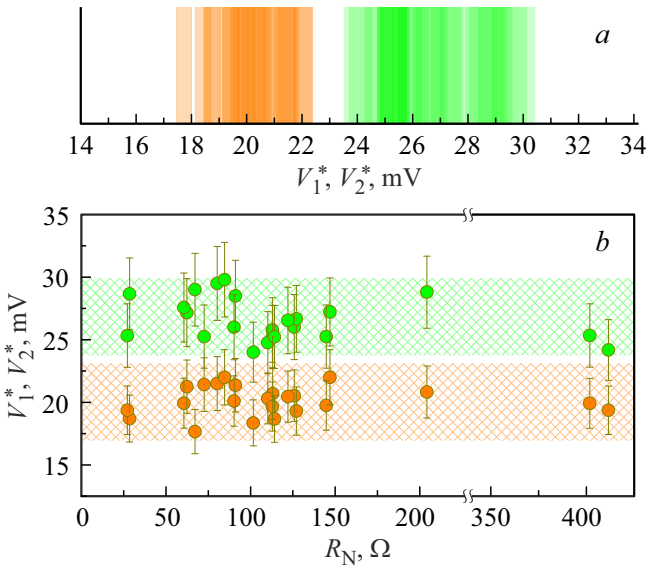

Figure 3. *a* — histogram of the positions of characteristic minima V_1^*, V_2* at $T = 4.2$ K of the residual nonlinearity $dI(V)/dV$ of the spectrum, unrelated directly with SC properties. For each contact studied, the pair of values V_1^*, V_2^* are shown as semitransparent columns of green and orange, respectively. The horizontal position of the area of maximum color intensity corresponds to the value most frequently observed in the experiment; the vertical axis does not matter. *b* — dependences V_1^*, V_2^* on normal contact resistance R_N obtained on samples of $NaFe_{1-x}Co_xAs$ of the undoped composition with $T_c \approx 19-22$ K from the same batch.

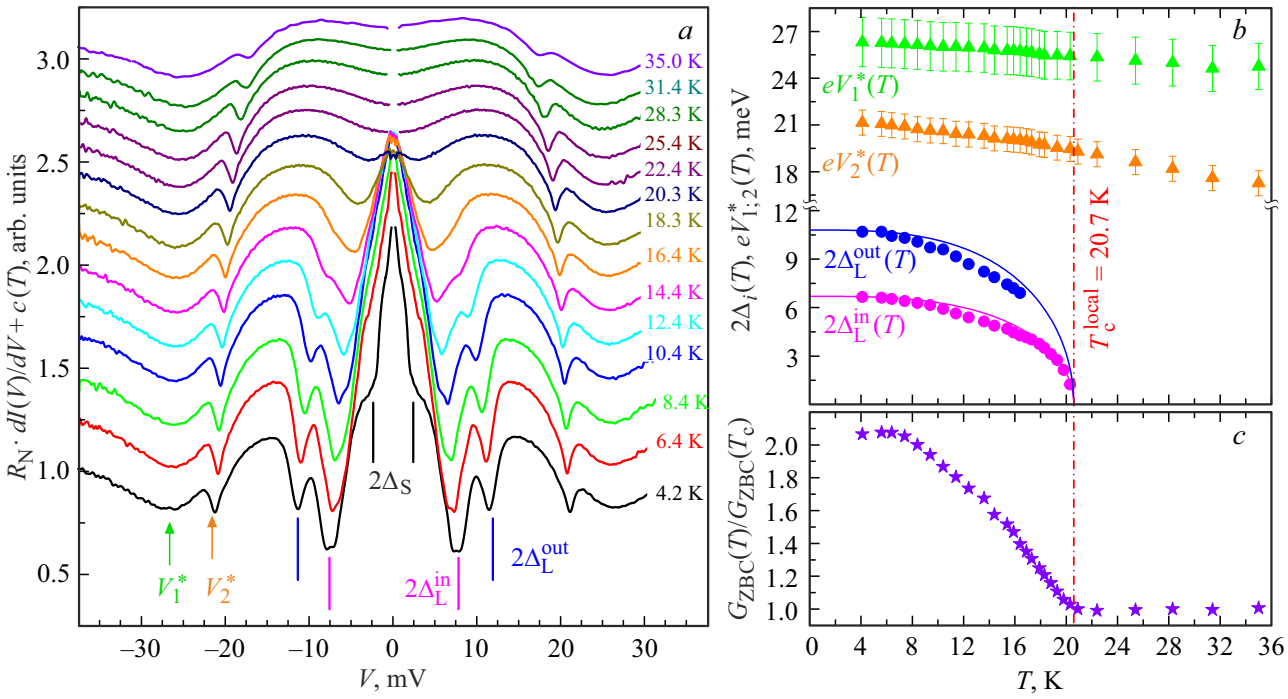

Figure 4. *a* — $dI(V)/dV$ is the tunneling contact spectrum measured at $4.2\,\text{K} \le T \le 35\,\text{K}$ in the superconducting (ScS) and normal (NcN) states. Local critical temperature $T_c^{local} \approx 20.7\,\text{K}$. The spectra are manually shifted vertically for convenience. Vertical dashes at $T = 4.2\,\text{K}$ mark the position of the fundamental Andreev features from three SC order parameters $2\Delta_L^{out} \approx 11.3\,\text{meV}$, $2\Delta_L^{in} \approx 7.5\,\text{meV}$, $2\Delta_S \approx 2.6\,\text{meV}$. The arrows at $T = 4.2\,\text{K}$ show the position of the characteristic minima of the residual nonlinearity of the $dI(V)/dV$-spectrum, which is not directly related to the SC properties: $eV_1^* \approx 26.6\,\text{meV}$, $eV_2^* \approx 21.2\,\text{meV}$. *b* — temperature dependences of the SC order parameters $2\Delta_L^{out,in}(T)$ (circles; single-band BCS-like functions are shown by solid lines for comparison) and the positions of the minima $eV_{1,2}^*(T)$ (triangles). A dotted line separates the SC area at $T < T_c^{local}$ and the normal state area. *c* — temperature dependence of conductance at zero bias $G_{ZBC}(T)$, normalized to its value at T_c (stars).

characteristic minima V_1^* and V_2^* (triangles in Figure 4, *b*) decrease monotonously both above and below T_c: in particular, the dependencies $V_{1,2}^*(T)$ do not repeat the shape of $\Delta_L^{in,out}(T)$ at $T < T_c$ and do not show any features at $T = T_c$. It is safe to conclude that these minima are not related to the properties of the superconducting subsystem. The temperature dependence of the conductance of this contact at zero bias $G_{ZBC}(T)$ is shown for comparison in Figure 4, *c*. A rather rapid decrease of G_{ZBC} is observed in the SC-state with the increase of the temperature due to a decrease in the amplitude of the „foot“, determined by the temperature dependences of superconducting gaps in accordance with the predictions in Ref. [53]. $G_{ZBC}(T)$ almost does not change in the normal state, at $T > T_c$ and with an increase of temperature to 36 K, confirming that the studied contact was in a semiballistic regime [54].

Figure 5, *a* shows the $dI(V)/dV$-spectrum of a tunneling SNINS contact created in another sample from the same batch and measured over a wider temperature range of $4.2\,\text{K} \le T \le 60.1\,\text{K}$ in a superconducting and normal state. The spectrum obtained at a temperature of 4.2 K shows a peak of dynamic conductance of G_{ZBC} at $eV = 0$, and the Andreev gap structure is represented by minima at small biases of $V \approx 4\,\text{mV}$, presumably from a small superconducting gap. The influence of the broadening parameter Γ can be assumed as the reason for the strongly suppressed amplitude of the Andreev features from a large gap. The observed features associated with Andreev reflections disappear after reaching $T_c^{local} \approx 22\,\text{K}$. The minima of residual nonlinearity at $V_1^* \approx 28.8\,\text{mV}$, $V_2^* \approx 18.8\,\text{mV}$, on the contrary, are observed up to the temperature of $T \approx 57\,\text{K} \gg T_c$. When the temperature $T = 60.1\,\text{K}$ is reached (the upper curve in Figure 5, *a*) at $dI(V)/dV$, the spectrum and the CVC are linearized.

As the temperature increases, the features at V_1^* is significantly smeared, which makes it difficult to study the dependence of its actual position on temperature. Figure 5, *b* shows the temperature dependence of the position of a sharper minimum of the nonlinearity of the normal state $V_2^*(T)$. It can be seen that the bias V_2^* decreases monotonously with temperature: from $V_2^*(0) \approx 18.8\,\text{mV}$ to $V_2^*(58\,\text{K}) \approx 10\,\text{mV}$.

The increased conductance at low bias (unrelated to the Andreev „foot“) persists in spectra up to $T \approx 60\,\text{K}$. Figure 5, *c* shows the temperature dependence of the reverse conductance of the studied tunneling contact at zero bias $1/G_{ZBC}$. In the superconducting region of $4.2\,\text{K} < T < T_c^{local} \approx 22\,\text{K}$ the value of $1/G_{ZBC}(T)$ increases with the growth of T according to the predictions in

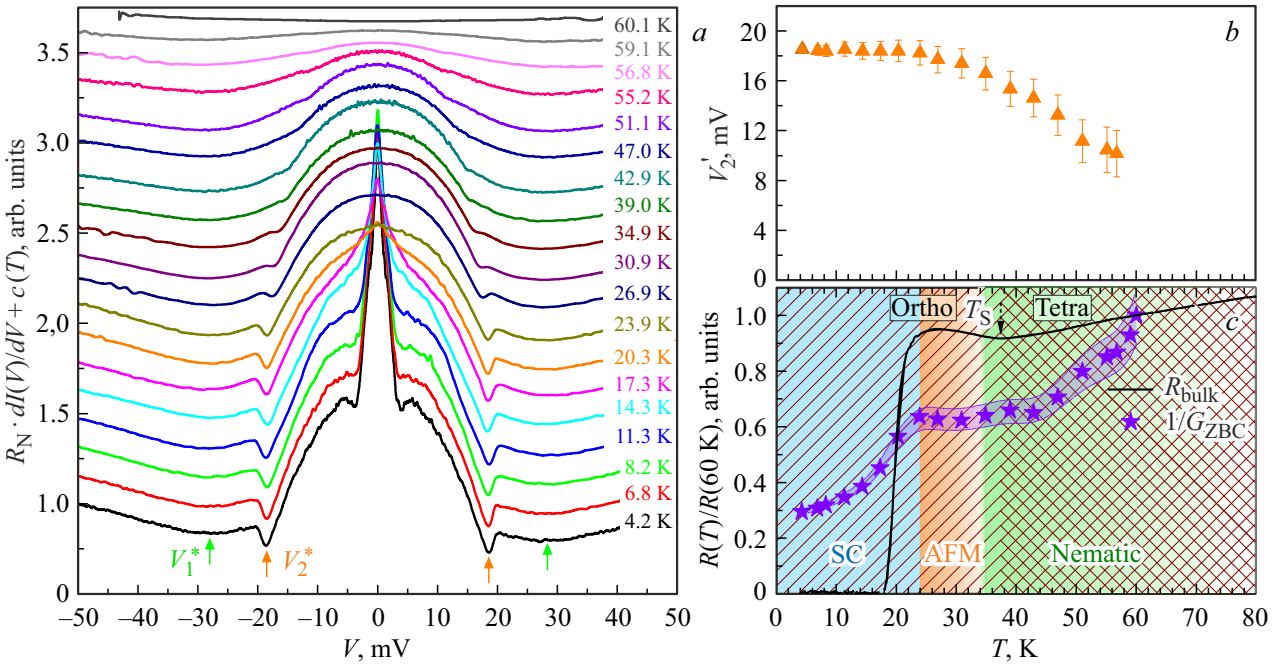

Figure 5. *a* — $dI(V)/dV$-spectrum of the tunneling contact measured at temperatures of $4.2\,\mathrm{K} \le T \le 60.1\,\mathrm{K}$ in the superconducting (ScS) and normal (NcN) states. Local critical temperature $T_c^{local} \approx 22\,\mathrm{K}$. The spectra are manually shifted vertically for convenience. The arrows at $T = 4.2\,\mathrm{K}$ mark the position of the characteristic minima of the residual nonlinearity of the $dI(V)/dV$-spectrum, which is not directly related to the SC properties: $V_1^* \approx 28.8\,\mathrm{mV}$, $V_2^* \approx 18.8\,\mathrm{mV}$. *b* — temperature dependence of the minimum position $V_{1,2}^*(T)$ (triangles). *c* — temperature dependence of the inverse conductance of the contact at zero bias $1/G_{ZBC}(T)$ (stars) and the bulk resistance of a single crystal $R_{bulk}(T)$ (solid black curve). Both values are normalized to their value at $T = 60\,\mathrm{K}$. The arrows indicate the temperatures of the structural phase transition $T_S \approx 37\,\mathrm{K}$, corresponding to the minimum on the dependence $R_{bulk}(T)$. The boundary of the nematic phase $T_{nem} \approx 55-80\,\mathrm{K}$ is marked according to the data in Refs. [12,14,16,17,33].

Ref. [53]. Above T_c and up to $T = 44\,\mathrm{K}$ the inverse conductance of the contact $1/G_{ZBC}(T)$ does not change within the experimental error. Starting from the temperature $T \approx 44\,\mathrm{K}$ in Figure 5, *a*, there is a gradual linearization of the spectra and a monotonous smearing of the conduction maximum at small bias voltages, corresponding to an increase in the $1/G_{ZBC}(T)$ contact in Figure 5, *c* by about 40% in the temperature range of $T = 44-60\,\mathrm{K}$.

4. Discussion

Before proceeding to the discussion of the most probable physical causes of the detected nonlinearity of the $dI(V)/dV$-spectra, let us once again consider possible parasitic effects.

The minima of the nonlinearity of the $dI(V)/dV$ spectrum at bias $V_{1,2}^*$ cannot be caused by overheating of the contact area during the flowing of the measuring current. First, the shape of the $dI(V)/dV$ spectrum of the contact in the thermal regime, which is subject to overheating (Figure 2 in [41]), which we modeled earlier, does not correspond to the one observed in the experiment. Secondly, in the thermal regime, the inverse conductance of the contact $1/G_{ZBC}(T)$ would repeat the course of the bulk resistance of the sample $R(T)$ (the black solid line in Figure 5, *c*), which contains the minimum at $T = T_s$ associated with the structural phase transition characteristic for underdoped compositions $NaFe_{1-x}Co_xAs$. On the contrary, as mentioned above, $G_{ZBC}(T) \approx \mathrm{const}$ in a wide range of temperatures $T > T_c$ and up to $T = 44\,\mathrm{K}$ means that there is no overheating of the contact area [54].

The processes of electron backscattering on nonequilibrium phonons can also be excluded from consideration. It is known that for ballistic contacts, such processes in the contact region lead to a slight (with the amplitude less than 10% of G_N [55]) drop in $dI(V)/dV$ with the increase of the bias voltage, whereas the experimental spectra obtained, on the contrary, demonstrate an increase in differential conductance in the region of bias $V > V_1^*$, and the amplitude of the observed nonlinearity $dI(V)/dV$ in the minimum region V_2^* reaches the value of 40% of G_N.

Also, the observed nonlinearity cannot be the result of geometric resonances in the contact region or random effects, since both the shape and position of the characteristic features of the spectra are reproduced and do not depend on the normal resistance of the contact, therefore, on its planar size (Figure 2). Thus, the observed effect is due to the internal, bulk properties of $NaFe_{1-x}Co_xAs$ undoped compounds. Since $dI(V)/dV$-spectra of tunneling contacts reproducibly demonstrate a maximum conductance

at small biases in $NaFe_{1-x}Co_xAs$ (with the exception of the $dI(V)/dV$-spectrum in Figure 1, which shows a slight decrease in the conductance in the center can be explained by local overheating), the pseudogap nature of the observed nonlinearity should be excluded.

Having considered the above arguments, it is possible to conclude that the presence of features of the density of electronic states $N(E)$ near the Fermi level in accordance with the classical approach is one of the probable causes of the nonlinearity of the $dI(V)/dV$-spectrum, unrelated to superconducting properties [52]. Unfortunately, detailed calculations or experimental data on the energy distribution of $N(E)$ in $NaFe_{0.979}Co_{0.021}As$ are currently not available in the literature, which complicates the calculation of the tunnel current and conductance using the formula (1) and, therefore, direct verification of this assumption. The observed temperature change in the shape of the residual nonlinearity of the spectrum (a gradual shift of the positions of the minima V_1^* and V_2^* towards zero, a decrease of G_{ZBC}, see Figs. 4 and 5) does not contradict the movement of bands with a temperature [6,7,30,31], which is not typical for classical materials. However, it is safe to say that these features of the $dI(V)/dV$ spectra cannot be caused by the renormalization of $N(E)$ to spin resonance, since the latter occurs only in the superconducting state at $T < T_c$ [56].

The form of residual nonlinearity of $dI(V)/dV$-spectra of tunneling NcN contacts in $NaFe_{0.979}Co_{0.021}As$ (Figures $1, b$ and $2, b$) does not repeat that in the pnictides $Ba(Fe,Ni)_2As_2$, which we observed earlier in a wide range of doping [36,37].

According to measurements of the resistance anisotropy in the ab-plane [14] and results of nuclear magnetic resonance studies [12] performed for $NaFe_{1-x}Co_xAs$ in a wide range of doping, the temperature of the nematic transition of the electronic subsystem for compositions with $x \approx 0.009-0.01$ (close to $x \approx 0.0094$ studied in this work) is $T_{nem} \approx 60-80\,K > T_s$. Similar estimates of $T_{nem} \approx 55-75\,K$ were obtained for the NaFeAs stoichiometric composition [16,17,33]. Since our experiment studied single crystals of the composition $Na_{0.69}Fe_{1.048}Co_{0.0094}As$ with a noticeable deficiency of sodium and a slight excess of iron, their phase diagram of electron substitution (Fe,Co) and characteristic phase temperatures may differ slightly from those for $NaFe_{1-x}Co_xAs$ samples. Nevertheless, a qualitative comparison can be made.

It is interesting to note that the temperature $T^* \approx 60\,K$ of linearization of the $dI(V)/dV$-spectrum according to Figure $5, c$ falls within the general temperature range of the nematic transition $T_{nem} \approx 55-80\,K$, estimated in Refs. [12,14,16,17,33] for underdoped and stoichiometric compounds. Thus, it can be assumed that the observed effect is related to the renormalization of the density of electronic states near the Fermi level caused by the nematic nature of the electronic subsystem.

We also note the reproducible absence of a similar nonlinearity above T_c on the CVC and $dI(V)/dV$-spectra of break-junctions in samples of the overdoped composition $NaFe_{0.955}Co_{0.045}As$ and in LiFeAs single crystals (which are known to lack a nematic phase [15,57], grown in a similar way and studied by us earlier [58,59]. For a more detailed analysis of the nature of the nonlinearity of $dI(V)/dV$spectra, it is necessary to determine its evolution with changes in electron doping in the parent substance NaFeAs and undoped $NaFe_{1-x}Co_xAs$ compositions, which seems to be the purpose of further studies.

5. Conclusion

The features of $I(V)$ and $dI(V)/dV$-characteristics of tunneling break-junctions created in single crystals of nominal underdoped composition $NaFe_{0.979}Co_{0.021}As$, in the superconducting and normal state, have been studied. Strong residual nonlinearity was reproducibly observed above T_c on $dI(V)/dV$-spectra, containing minima at biases $V_1^* \approx 20\,mV$, $V_2^* \approx 27\,mV$, and a maximum of dynamic conductance at small biases, which disappeared at $T^* \approx 60\,K$. The intrinsic nature of the observed effect and its possible relation to the nematic nature of the electronic subsystem are shown. The effect of gradual linearization of the $dI(V)/dV$-spectrum and reduction of $G_{ZBC}(T)$ occurred at a temperature of $T \approx 44\,K$, perfectly consistent with the temperature of the nematic transition T_{nem} according to Ref. [14].

Acknowledgments

The authors would like to thank M.M. Korshunov for useful discussions. This study was supported by the project No. 22-72-10082 of the Russian Science Foundation.

Conflict of interest

The authors declare that they have no conflict of interest.

References

[1] J.H. Tapp, Z. Tang, B. Lv, K. Sasmal, B. Lorenz, P.C.W. Chu, A.M. Guloy. Phys. Rev. B **78**, *6*, 060505(R) (2008).
[2] D.R. Parker, M.J.P. Smith, T. Lancaster, A.J. Steele, I. Franke, P.J. Baker, F.L. Pratt, M.J. Pitcher, S.J. Blundell, S.J. Clarke. Phys. Rev. Lett. **104**, *5*, 057007 (2010).
[3] Y. Kamihara, H. Hiramatsu, M. Hirano, R. Kawamura, H. Yanagi, T. Kamiya, H. Hosono, J. Am. Chem. Soc. **128**, *31*, 10012 (2006).
[4] M.D. Watson, S. Aswartham, L.C. Rhodes, B. Parrett, H. Iwasawa, M. Hoesch, I. Morozov, B. Büchner, T.K. Kim. Phys. Rev. B **97**, *3*, 035134 (2018).
[5] T.E. Kuzmicheva, S.A. Kuzmichev. JETP Lett. **114**, *10*, 630 (2021).
[6] R.S. Dhaka, S.E. Hahn, E. Razzoli, R. Jiang, M. Shi, B.N. Harmon, A. Thaler, S.L. Bud'ko, P.C. Canfield, A. Kaminski. Phys. Rev. Lett. **110**, *6*, 067002 (2013).

[7] L.L. Lev, T.E. Kuzmicheva, S.A. Kuzmichev, A.M. Lebedev, V.G. Nazin, R.G. Chumakov, A.I. Shilov, E.O. Rahmanov, I.V. Morozo. Moscow Univ. Bull. Phys. **79**, *1*, 46 (2024).
[8] H. Ghosh, S. Sen, A. Ghosh. J. Phys. Chem. Solids **102**, *7*, 157 (2017).
[9] J.D. Wright, T. Lancaster, I. Franke, A.J. Steele, J.S. Müller, M.J. Pitcher, A.J. Corkett, D.R. Parker, D.G. Free, F.L. Pratt, P.J. Baker, S.J. Clarke, S.J. Blundell. Phys. Rev. B **85**, *5*, 054503 (2012).
[10] A. Martinelli, F. Bernardini, S. Massidda. Comptes Rendus Physique **17**, *1−2*, 5 (2015).
[11] R.M. Fernandes, A.V. Chubukov, J. Schmalian. Nature Phys. **10**, *2*, 97 (2014).
[12] R. Zhou, L.Y. Xing, X.C. Wang, C.Q. Jin, G.-Q. Zheng. Phys. Rev. B **93**, *6*, 060502(R) (2016).
[13] P. Cai, W. Ruan, X. Zhou, C. Ye, A. Wang, X. Chen, D.-H. Lee, Y. Wang. Phys. Rev. Lett. **112**, *12*, 127001 (2014).
[14] Q. Deng, J. Liu, J. Xing, H. Yang, H.-H. Wen. Phys. Rev. B **91**, *2*, 020508(R) (2015).
[15] E.P. Rosenthal, E.F. Andrade, C.J. Arguello, R.M. Fernandes, L.Y. Xing, X.C. Wang, C.Q. Jin, A.J. Millis, A.N. Pasupathy. Nature Phys. **10**, *3*, 225 (2014).
[16] Y. Zhang, C. He, Z.R. Ye, J. Jiang, F. Chen, M. Xu, Q.Q. Ge, B.P. Xie, J. Wei, M. Aeschlimann, X.Y. Cui, M. Shi, J.P. Hu, D.L. Feng. Phys. Rev. B **85**, *8*, 085121 (2012).
[17] S.-H. Baek, D. Bhoi, W. Nam, B. Lee, D.V. Efremov, B. Büchner, K.H. Kim. Nature Commun. **9**, *1*, 2139 (2018).
[18] X. Lu. Phase Diagram and Magnetic Excitations of $BaFe_{2-x}Ni_xAs_2$: A Neutron Scattering Study. Springer, Singapore (2017).
[19] J.-H. Chu, J.G. Analytis, K. De Greve, P.L. McMahon, Z. Islam, Y. Yamamoto, I.R. Fisher. Sci. **329**, *5993*, 824 (2010).
[20] X. Lu, J.T. Park, R. Zhang, H. Luo, A.H. Nevidomskyy, Q. Si, P. Dai. Sci. **345**, *6197*, 657 (2014).
[21] M.P. Smylie, K. Willa, J.K. Bao, K. Ryan, Z. Islam, H. Claus, Y. Simsek, Z. Diao, A. Rydh, A.E. Koshelev, W.K. Kwok, D.Y. Chung, M.G. Kanatzidis, U. Welp. Phys. Rev. B **98**, *10*, 104503 (2018).
[22] V.S. Stolyarov, A. Casano, M.A. Belyanchikov, A.S. Astrakhantseva, S.Y. Grebenchuk, D.S. Baranov, I.A. Golovchanskiy, I. Voloshenko, E.S. Zhukova, B.P. Gorshunov, A.V. Muratov, V.V. Dremov, L.Y. Vinnikov, D. Roditchev, Y. Liu, G.-H. Cao, M. Dressel, E. Uykur. Phys. Rev. B **98**, *14*, 140506(R) (2018).
[23] A. Kreisel, B.M. Andersen, P.O. Sprau, A. Kostin, J.C. Séamus Davis, P.J. Hirschfeld. Phys. Rev. B **95**, *17*, 174504 (2017).
[24] M.M. Korshunov, Yu.N. Togushova. JETP Lett. **119**, *4*, 310 (2024).
[25] P.O. Sprau, A. Kostin, A. Kreisel, A.E. Böhmer, V. Taufour, P.C. Canfield, S. Mukherjee, P.J. Hirschfeld, B.M. Andersen, J.C. Séamus Davis. Sci. **357**, *6346*, 75 (2017).
[26] R.M. Fernandes, A.V. Chubukov, J. Knolle, I. Eremin, J. Schmalian. Phys. Rev. B **85**, *2*, 024534 (2012).
[27] Y. Gallais, R.M. Fernandes, I. Paul, L. Chauviére, Y.-X. Yang, M.-A. Méasson, M. Cazayous, A. Sacuto, D. Colson, A. Forget. Phys. Rev. Lett. **111**, *26*, 267001 (2013).
[28] H. Kontani, Y. Yamakawa. Phys. Rev. Lett. **113**, *4*, 047001 (2014).
[29] A.A. Kordyuk, V.B. Zabolotnyy, D.V. Evtushinsky, A.N. Yaresko, B. Büchner, S.V. Borisenko. J. Supercond. Nov. Magn. **26**, *9*, 2837 (2013).
[30] T. Sonobe, T. Shimojima, A. Nakamura, M. Nakajima, S. Uchida, K. Kihou, C.H. Lee, A. Iyo, H. Eisaki, K. Ohgushi, K. Ishizaka. Sci. Rep. **8**, *1*, 2169 (2018).
[31] T. Shimojima, T. Sonobe, W. Malaeb, K. Shinada, A. Chainani, S. Shin, T. Yoshida, S. Ideta, A. Fujimori, H. Kumigashira, K. Ono, Y. Nakashima, H. Anzai, M. Arita, A. Ino, H. Namatame, M. Taniguchi, M. Nakajima, S. Uchida, Y. Tomioka, T. Ito, K. Kihou, C.H. Lee, A. Iyo, H. Eisaki, K. Ohgushi, S. Kasahara, T. Terashima, H. Ikeda, T. Shibauchi, Y. Matsuda, K. Ishizaka. Phys. Rev. B **89**, *4*, 045101 (2014).
[32] S. Onari, H. Kontani. Phys. Rev. Res. **2**, *4*, 042005(R) (2020).
[33] C. He, Y. Zhang, B.P. Xie, X.F. Wang, L.X. Yang, B. Zhou, F. Chen, M. Arita, K. Shimada, H. Namatame, M. Taniguchi, X.H. Chen, J.P. Hu, D.L. Feng. Phys. Rev. Lett. **105**, *11*, 117002 (2010).
[34] Q.Q. Ge, Z.R. Ye, M. Xu, Y. Zhang, J. Jiang, B.P. Xie, Y. Song, C.L. Zhang, P. Dai, D.L. Feng. Phys. Rev. X **3**, *1*, 011020 (2013).
[35] P. Szabó, Z. Pribulová, G. Pristáš, S.L. Bud'ko, P.C. Canfield, P. Samuely. Phys. Rev. B **79**, *1*, 012503 (2009).
[36] I.A. Nikitchenkov, A.D. Ilina, V.M. Mikhailov, K.S. Pervakov, V.A. Vlasenko, S.A. Kuzmichev, T.E. Kuzmicheva. Moscow Univ. Bull. Phys. **78**, *4*, 521 (2023).
[37] I.A. Nikitchenkov, S.A. Kuzmichev, A.D. Ilyina, K.S. Pervakov, V.A. Vlasenko, T.E. Kuzmicheva. ZhETF, **166**, *6*, 834 (2024). (in Russian).
[38] H.Z. Arham, L.H. Greene. Current Opinion. Solid State. Mater. Sci. **17**, *2*, 81 (2013).
[39] M.J. Lawler, D.G. Barci, V. Fernández, E. Fradkin, L. Oxman. Phys. Rev. B **73**, *8*, 085101 (2006).
[40] W.-C. Lee, P.W. Phillips. Phys. Rev. B **86**, *24*, 245113 (2012).
[41] S.A. Kuzmichev, I.V. Morozov, A.I. Shilov, E.O. Rakhmanov, T.E. Kuzmicheva. JETP Lett. **117**, *8*, 612 (2023).
[42] L. Morgun, S. Kuzmichev, I. Morozov, A. Degtyarenko, A. Sadakov, A. Shilov, I. Zhuvagin, Y. Rakhmanov, T. Kuzmicheva. Mater. **16**, *19*, 6421 (2023).
[43] S.A. Kuzmichev, T.E. Kuzmicheva. Low Temperature Phys. **42**, *11*, 1008 (2016).
[44] J. Moreland, J.W. Ekin. J. Appl. Phys. **58**, *10*, 3888 (1985).
[45] Z. Popovic, S.A. Kuzmichev, T.E. Kuzmicheva. J. Appl. Phys. **128**, 013901 (2020).
[46] G.E. Blonder, M. Tinkham, T.M. Klapwijk. Phys. Rev. B **25**, *7*, 4515 (1982).
[47] M. Octavio, M. Tinkham, G.E. Blonder, T.M. Klapwijk. Phys. Rev. B **27**, *11*, 6739 (1983).
[48] R. Kümmel, U. Gunsenheimer, R. Nicolsky. Phys. Rev. B **42**, *7*, 3992 (1990).
[49] R.C. Dynes, V. Narayanamurti, J.P. Garno. Phys. Rev. Lett. **41**, *21*, 1509 (1978).
[50] Yu.G. Naidyuk, K. Gloos. Low Temperature Phys. **44**, *4*, 343 (2018).
[51] J. Fink, J. Nayak, E.D.L. Rienks, J. Bannies, S. Wurmehl, S. Aswartham, I. Morozov, R. Kappenberger, M.A. ElGhazali, L. Craco, H. Rosner, C. Felser, B. Büchner. Phys. Rev. B **99**, *24*, 245156 (2019).
[52] I. Giaever, K. Megerle. Phys. Rev. **122**, *4*, 1101 (1961).
[53] U. Gunsenheimer, A.D. Zaikin. Phys. Rev. B **50**, *9*, 6317 (1994).

[54] Yu.V. Sharvin. JETP **21**, *3*, 655 (1965).
[55] N.L. Bobrov. Phys. — Uspekhi **63**, *11*, 1072 (2020).
[56] M.M. Korshunov, S.A. Kuzmichev, T.E. Kuzmicheva. Mater. **15**, *17*, 6120 (2022).
[57] M. Wissmann, F. Caglieris, X. Hong, S. Aswartham, A. Vorobyova, I. Morozov, B. Büchner, C. Hess. Phys. Rev. B **106**, *5*, 054508 (2022).
[58] S. Kuzmichev, A. Muratov, S. Gavrilkin, I. Morozov, A. Shilov, Y. Rakhmanov, A. Degtyarenko, T. Kuzmicheva. Eur. Phys. J. Plus **139**, *1*, 74 (2024).
[59] S. Kuzmichev, T. Kuzmicheva, I. Morozov, A. Boltalin, A. Shilov. Discover Appl. Sci. **4**, *6*, 189 (2022).

Translated by A.Akhtyamov